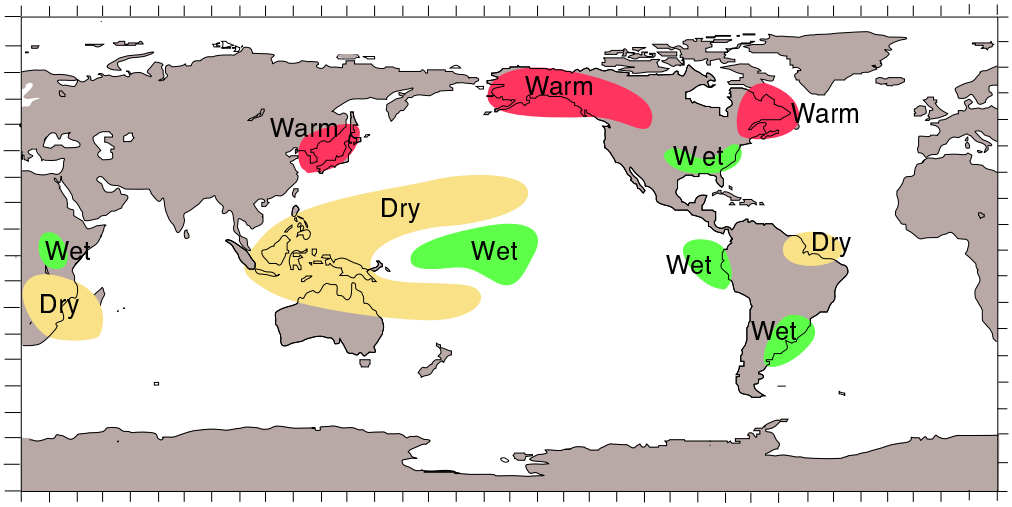

Figure 20. Summary of the major large-scale climate anomalies associated with the warm phase of the ENSO cycle during the Northern Hemisphere winter.

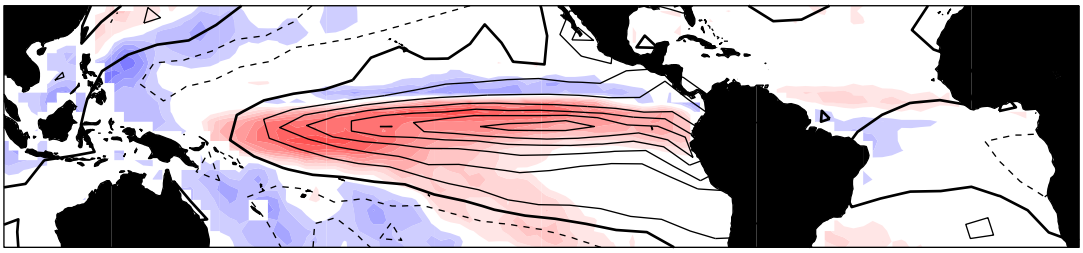

Figure 21. Sea surface temperature anomalies (contour interval 0.2°C) and ocean rainfall anomalies during a typical warm episode of the ENSO cycle. Enhanced rainfall, indicated by the red shading, is observed over the region of above-normal sea surface temperature, and reduced rainfall, indicated by the blue shading, is observed throughout much of the surrounding region and over the tropical Atlantic adjacent to Northeast Brazil.

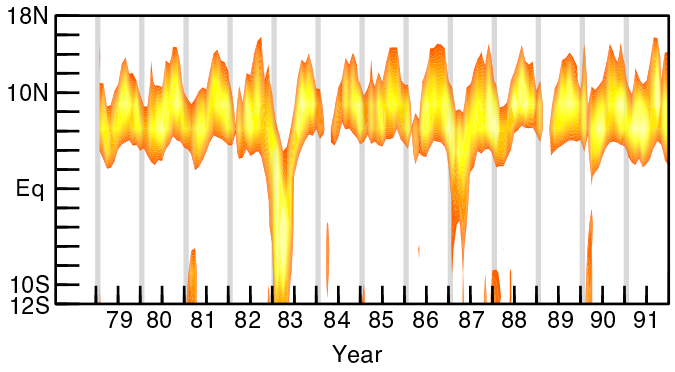

Figure 22. Time-latitude sections of the core of the heavy rainfall associated with the Pacific ITCZ, averaged over longitudes 180-110°W. Estimated rainfall amounts range from 20 cm per month for the orange up to ~50 cm per month for the yellow. Each year the ITCZ is closest to the equator from February through April. The rainy seasons of 1983 and 1987 fell within warm episodes of the ENSO cycle.

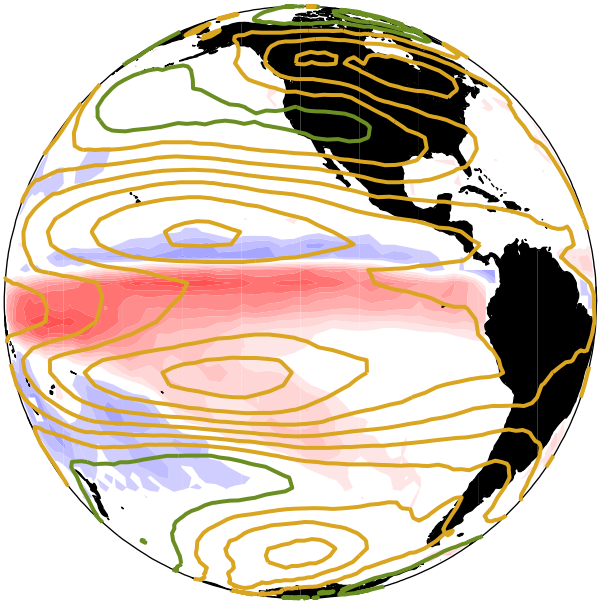

Figure 23. Anomalous rainfall observed during a typical warm episode of the ENSO cycle (colored shading, repeated from Fig. 21) shown with the corresponding pattern of anomalies in mean tropospheric temperature (contours: gold positive and green negative). The pair of temperature extrema straddling the equator in the eastern Pacific are warm anomalies, which correspond to anomalous anticyclonic gyres in the upper-tropospheric flow. These disturbances in the upper-level flow are responsible for the wide-ranging impacts of ENSO upon the climate of the Americas.

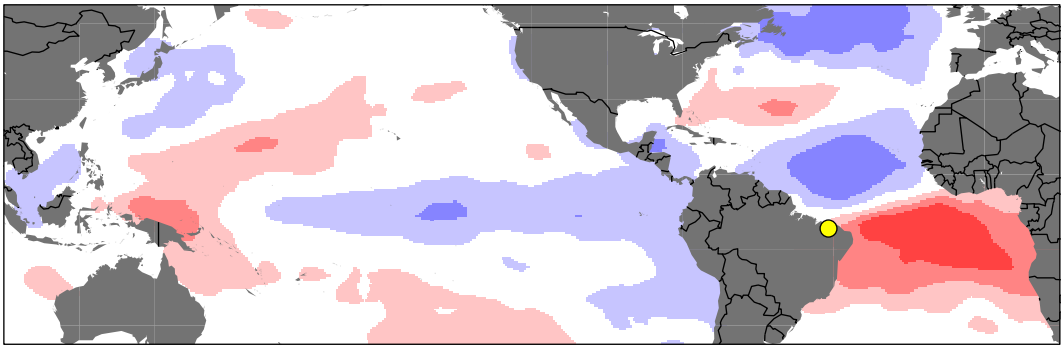

Figure 24. Correlation between average February through May precipitation in northeast Brazil (yellow dot) and sea surface temperature. Red (blue) shading indicates regions in which above-normal sea surface temperatures tend to be observed in conjunction with the above (below) normal rainfall in northeast Brazil. The strongest correlations are on the order of 0.7. Northeast Brazil rainfall tends to be more strongly correlated with Atlantic sea surface temperatures than with Pacific sea surface temperatures.

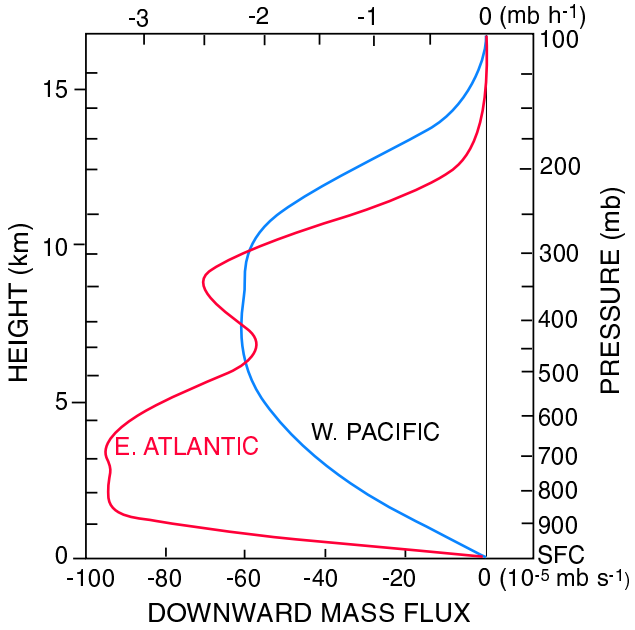

Figure 25. Contrasting vertical mass flux profiles in disturbed regions of the ITCZ in the eastern Atlantic and the "warm core" region of the western Pacific. In the ITCZ the low-level convergence (indicated by the large negative vertical derivative) is concentrated within the lowest 1.5 km, whereas in the western Pacific it is much weaker and extends all the way up to 5 km.

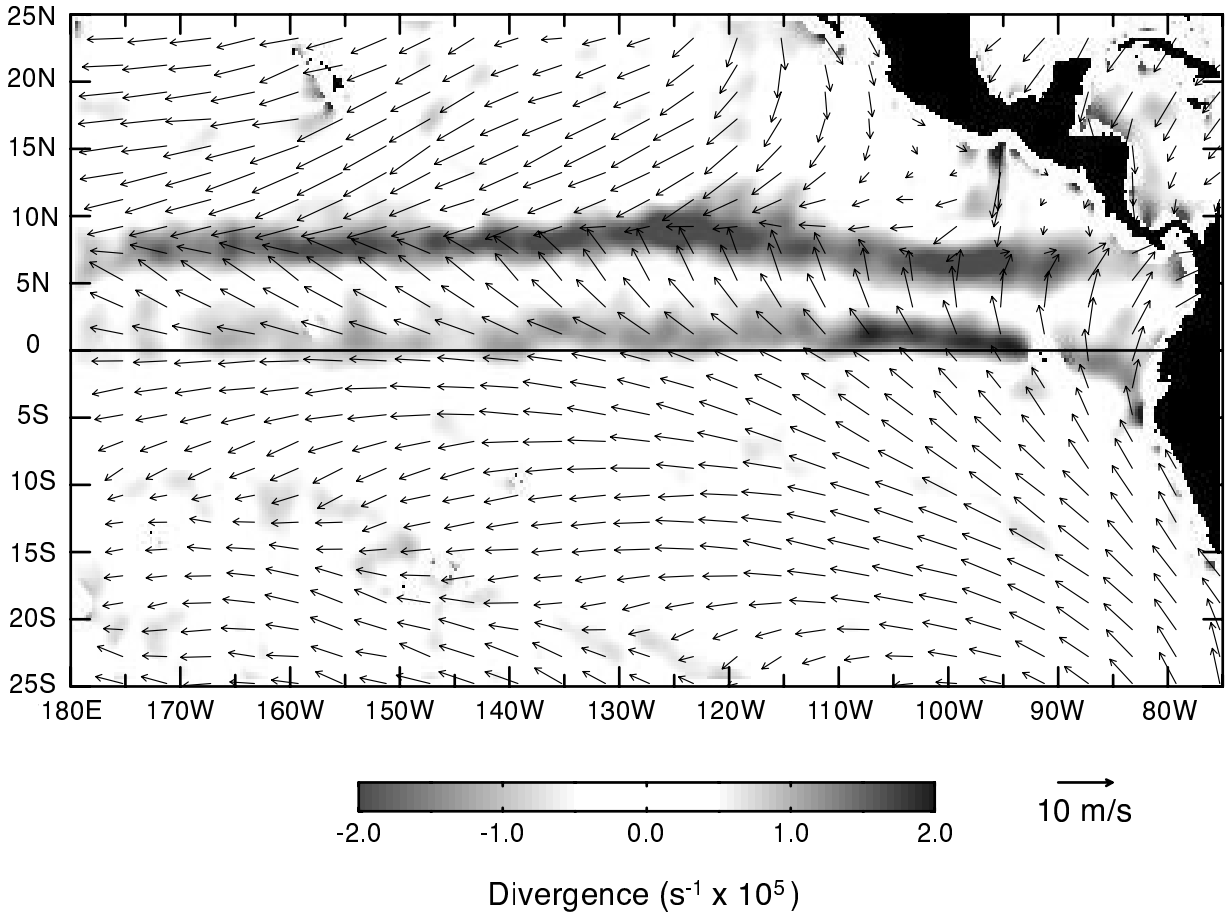

Figure 26. NASA QuikSCAT scatterometer 10-m vector wind averaged for November 1999 (vectors) and the corresponding divergence field. Red and blue denote convergence and divergence, respectively. Shading units in increments of 10^{-5} s^{-1}.

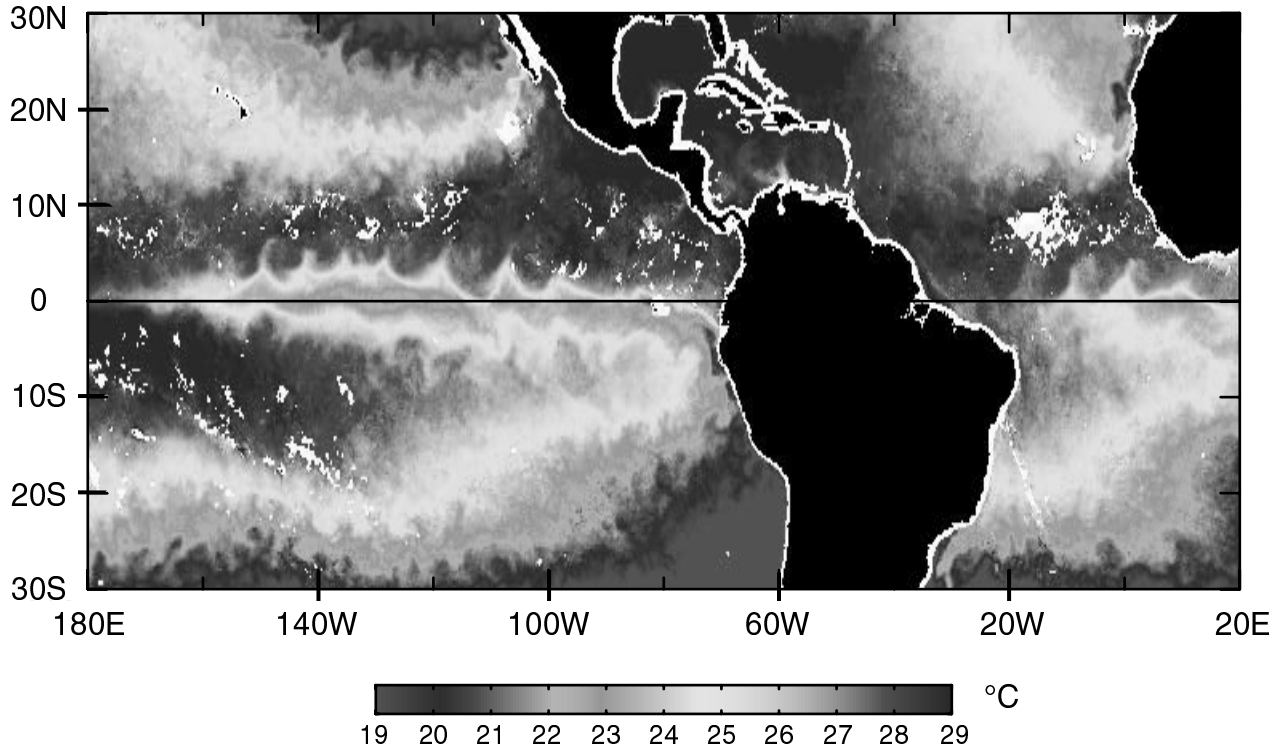

Figure 27. Three-day composite average maps of sea surface temperature for 11-13 July 1998, during a time of year when the equatorial Pacific and Atlantic are typically cool. The maps are based on measurements from a satellite microwave radiometer (TMI). White areas represent land or rain contamination. The sharp northern edge of the cold tongue is distorted by westward-propagating tropical instability waves which originate in the ocean, but produce a distinct signature in the fields of cloudiness and wind speed.

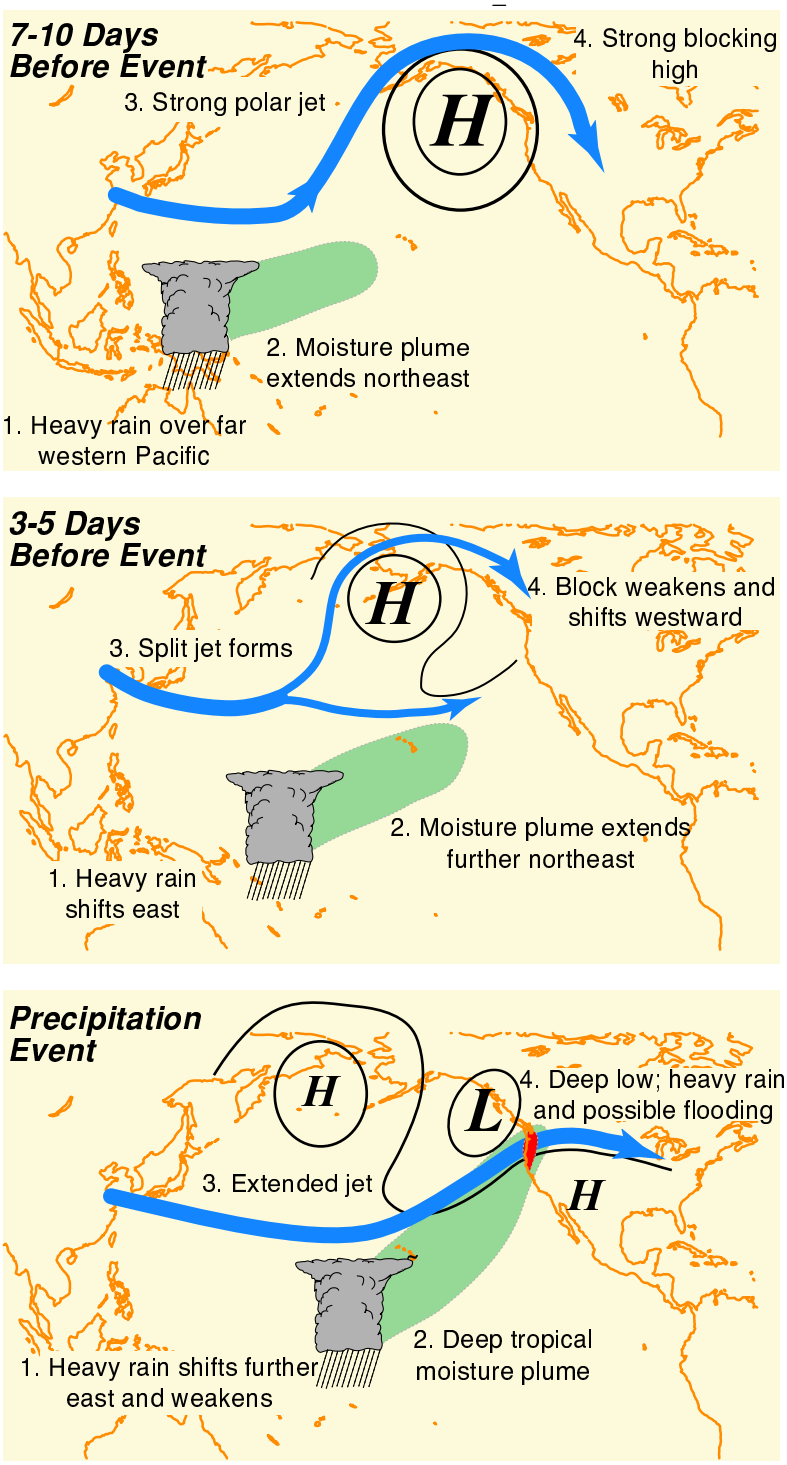

Figure 28. Typical wintertime weather anomalies preceding heavy precipitation events over the northwestern U.S.

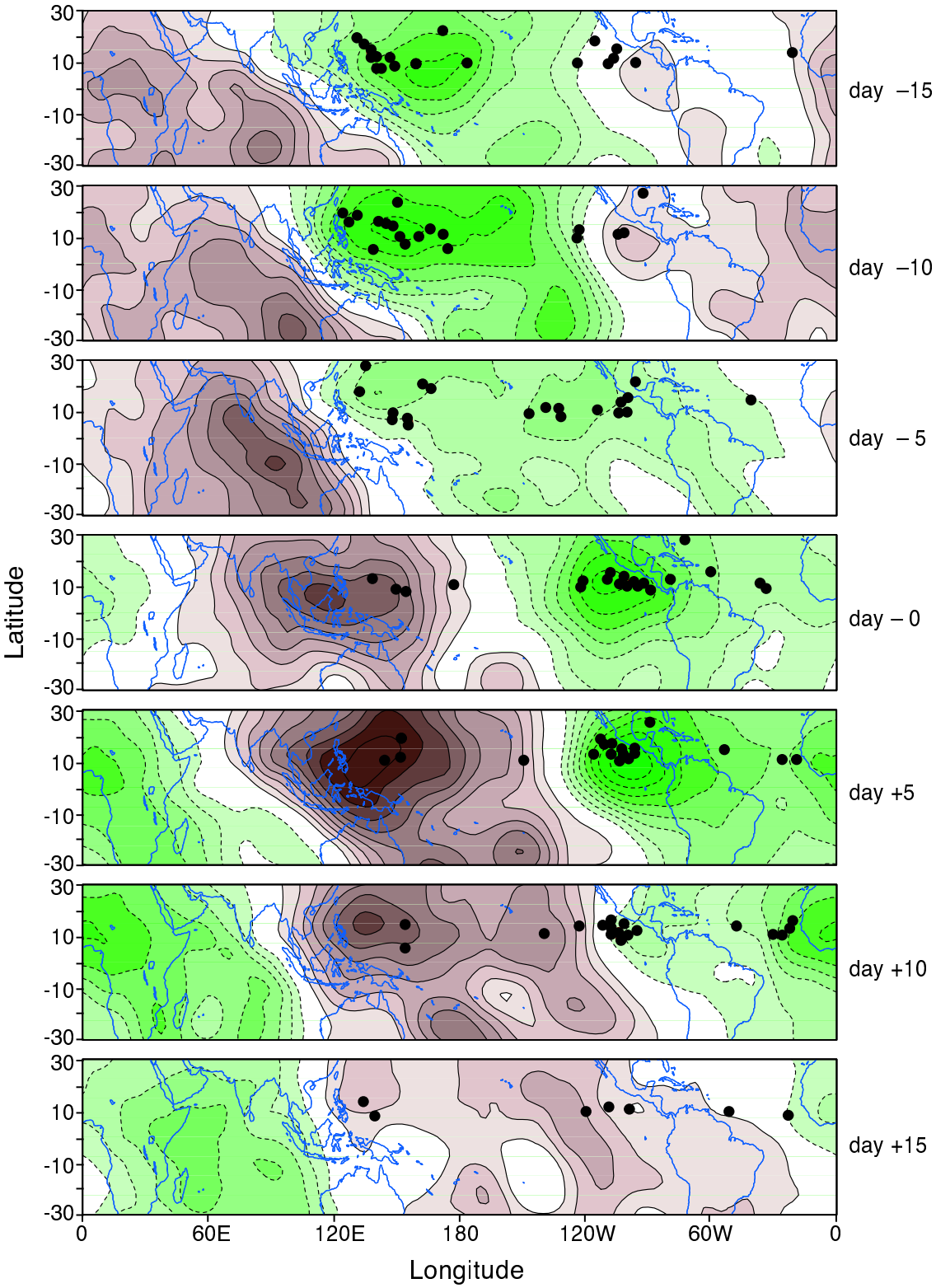

Figure 29. Composited evolution of 200 hPa velocity potential anomalies (10^6 m^2 s^{-1}) and points of origin of weather systems that developed into hurricanes or typhoons (●).